energies

MDPI

Article

A New Method for Calculating the Influx Index in Gas-Drive Reservoirs: A Case Study of the Kela-2 Gas Field

Donghuan Han [1,2,3,*], Tongwen Jiang [4], Wei Xiong [2], Shusheng Gao [2], Huaxun Liu [2], Liyou Ye [2], Wenqing Zhu [2] and Weiguo An [2]

[1] University of Chinese Academy of Sciences, Beijing 100049, China
[2] Research Institute of Petroleum Exploration and Development, PetroChina, Beijing 100083, China; xiongwei69@petrochina.com.cn (W.X.); gaoshusheng69@petrochina.com.cn (S.G.); liuhuaxun@petrochina.com.cn (H.L.); yeliyou69@petrochina.com.cn (L.Y.); zhuwengqing@petrolchina.com.cn (W.Z.); anweiguo69@petrochina.com.cn (W.A.)
[3] Institute of Porous Flow and Fluid Mechanics, Chinese Academy of Sciences, Langfang 065007, China
[4] Department of Science and Technology Management, PetroChina Company Limited, Beijing 100007, China; jiangtw-tlm@petrochina.com.cn
* Correspondence: handonghuan19@mails.ucas.ac.cn

Abstract: The calculation of the influx index is one of the most contentious issues in dynamic reserve evaluation of gas reservoirs' development. For the influx index, it is key to obtain information on the pore compressibility coefficient under realistic gas reservoir pressure. So far, little is known about the assessment of the pore compressibility coefficient at a laboratory scale. Here, we combine observations of gas flowmeter, ISCO booster pump, intermediate container, and rock samples to quantify the pore compressibility coefficient from the KL2-13 well in the Kela-2 reservoir. Additionally, the iterative method (combined the static and dynamic methods) is proposed based on the experimentally obtained pore compressibility coefficient (C_f), dynamic reserve (G), water body multiple (β), and material balance equation to calculate the influx index. The combined iterative method adjusts the values of G and N by comparing the results of the static and dynamic methods, and iteratively corrects C_f using a binary search method until the results of the static and dynamic methods are consistent. The results of our study reveal that the influx index calculated by the dynamic and static methods was consistent, and the gas production per unit pressure drop matched the actual production. These results strongly suggest that there exists a correlation between formation pressure and the influx index, wherein the latter exhibits a gradual decrease as the former decreases. Conversely, the displacement index of both the rock and connate water do not demonstrate a significant dependence on pressure. Furthermore, the impact of pressure on the pore compressibility factor and reservoir water compressibility factor appears to be minimal. These findings hold substantial implications for understanding the behavior of gas reservoirs under varying pressure conditions.

Keywords: influx index; Kela-2 reservoir; pore compressibility coefficient; dynamic reserve

Citation: Han, D.; Jiang, T.; Xiong, W.; Gao, S.; Liu, H.; Ye, L.; Zhu, W.; An, W. A New Method for Calculating the Influx Index in Gas-Drive Reservoirs: A Case Study of the Kela-2 Gas Field. *Energies* **2024**, *17*, 1076. https://doi.org/10.3390/en17051076

Academic Editor: Seung Gu Shin

Received: 21 December 2023
Revised: 1 February 2024
Accepted: 13 February 2024
Published: 23 February 2024

1. Introduction

Water invasion in gas reservoirs holds a significant proportion in the natural gas reserves. Upon encountering water in gas wells, the nearby formation transitions from single-phase natural gas flow to two-phase gas/water flow, leading to a reduction in the effective permeability of natural gas [1]. This results in a narrower range of pressure fluctuations in gas wells. Additionally, the continuous accumulation of reservoir water near the wellbore hampers the flow of natural gas, causing water blockage [2]. The majority of gas reservoirs in China's exploration and development phase are classified as water-invasion reservoirs to varying extents [3]. Among the various factors affecting the effectiveness of natural gas reservoir development, the type of drive mechanism is considered the most significant. According to the classification standards for natural

gas reservoirs, water-invasion gas reservoirs can be categorized as weak water-invasion, moderate water-drive, and strong water-invasion reservoirs, based on the energy of the water phase [4]. Different types of reservoirs exhibit distinct dynamic characteristics during development. Weak water-invasion gas reservoirs are typically closed systems, with occasional water production or even no water production from individual wells during the later stages of production, resulting in an influx index below 0.1 [5]. Moderate water-invasion gas reservoirs have relatively weaker water energy or smaller contact areas between the gas and water phases. Local water breakthroughs and limited water production usually occur in the mid-to-late stages of production, resulting in an influx index ranging from 0.1 to 0.3 [5]. Strong water-invasion gas reservoirs have a larger water phase, and during the early stages of development, excessive water production or water inundation can occur due to a high water/gas ratio and proximity to the gas/water interface [5]. These reservoirs exhibit high water production rates and shorter periods of stable gas production, with an influx index exceeding 0.3. Accurate evaluation of the influx index during the early stages of development is crucial for water-invasion gas reservoirs [6]. The driving energy in water-invasion reservoirs includes the expansion force of natural gas, the elastic energy of edge and bottom water, and the expansion force of rock and bound water [7]. The percentage of each driving energy component in the total driving energy is defined as the driving index [8].

The driving index reflects the magnitude of the energy contribution of various driving mechanisms in fluid flow [8]. For water-invasion gas reservoirs, the influx index is an important parameter for determining development strategies. According to the definition of the driving index, the influx index represents the proportion of the energy contributed by edge and bottom water in the total energy. The expression is as follows [8]:

$$WEDI = \frac{W_e}{G_p B_g + W_p B_w} \tag{1}$$

where $WEDI$ represents the influx index, dimensionless; W_e represents the cumulative water invasion, 10^4 m^3; G_p represents the cumulative gas production, 10^4 m^3; W_p represents the cumulative water production, 10^4 m^3; B_g represents the gas volumetric factor, dimensionless; B_w represents the formation water volumetric factor, dimensionless.

Based on the dynamic production of gas wells, cumulative gas production and cumulative water production are relatively easy-to-obtain parameters. However, the calculation of water invasion has always been a challenging aspect in the development of water-invasion gas reservoirs. Schilthuis proposed a method for calculating the water invasion of steady-state water encroachment based on Darcy's law [9]. Everdingen derived non-steady-state formulas applicable to radial and linear models for the aquifer [10]. Fetkovich developed the Fetkovich model, which can simulate the behavior of finite water encroachment layers [11]. To simplify calculations, the model assumed that water invasion could be described by productivity index, neglecting the influence of non-steady-state periods and directly considering pseudo-steady-state flow [11].

Most of the research on water invasion calculation in domestic studies is based on the material balance equation of water-invasion gas reservoirs [12]. According to the material balance equation of water-invasion gas reservoirs, the expression for water invasion is as follows [12]:

$$G_p B_g + W_p B_w = G(B_g - B_{gi}) + \Delta V_w + \Delta V_r + W_e \tag{2}$$

where G represents the dynamic reserves, 10^4 m^3; B_{gi} represents the gas volumetric factor at the original reservoir pressure, dimensionless; ΔV_r represents the compressibility volume of rock pores, 10^4 m^3; $G_p B_g$ is the underground volumes of cumulative gas production, m^3; $W_p B_w$ is the volumes of cumulative water production, m^3; $G(B_g - B_{gi})$ is expansion volumes of natural gas, m^3; ΔV_w is the expansion volumes of bound water, m^3; ΔV_r is the volumes pore compressibility, m^3.

The bound water expansion volume is defined as follows [12]:

$$\Delta V_w = GB_{gi}\int_P^{P_i}\left(\frac{S_{wi}C_w}{1-S_{wi}}\right)dp \tag{3}$$

The pore compressibility volume is defined as follows [12]:

$$\Delta V_r = GB_{gi}\int_P^{P_i}\left(\frac{C_f}{1-S_{wi}}\right)dp \tag{4}$$

where C_w represents the reservoir water compressibility factor, MPa^{-1}; C_f represents the pore compressibility factor, MPa^{-1}; S_{wi} represent the initial water saturation, %.

The uncertainty in determining the values of G and C_f severely affects the calculation of water invasion, influx index, and the ultimate recovery factor of gas reservoirs [13]. Various methods have been proposed for calculating the dynamic reserves of water-invasion gas reservoirs, such as the pressure drop method, decline curve analysis, and water-invasion performance curve method [14]. However, all these methods are based on the derivation of material balance equations. Bruns used the pressure drop method (also known as the P/Z curve method) derived from the material balance equation to determine dynamic reserves [15]. This research indicated that the shape and deviation direction of the P/Z relationship curve with cumulative gas production mainly depend on the magnitude of subsurface water energy, water properties, and the geometric shape of the water body [15]. The Cole curve, derived based on the material balance equation of the reservoir, can effectively distinguish between depleted gas reservoirs and water-invasion gas reservoirs and calculate the dynamic reserves of these two types of reservoirs [16].

There have been numerous studies on the dynamic reserves of water-invasion gas reservoirs in China as well [17]. Wang et al. proposed a new method for calculating the dynamic geological reserves and water invasion of water-invasion gas reservoirs by establishing an objective function using production data, such as reservoir pressure and cumulative production, applying the least squares method for automatic fitting [18]. Tang et al. introduced the material balance equation of water-invasion gas reservoirs and the static reservoir pressure from tests as constraints; established objective functions using production, flow pressure, and test reservoir pressure; fitted the dynamic production data; and obtained the dynamic reserves of the gas reservoirs as well as the water invasion [19]. Based on the mechanism of water pressure drop caused by reservoir pressure decline, pore contraction of water-bearing rocks, and elastic expansion of water in the reservoir, Zhang et al. derived a water invasion calculation model and established a new method for calculating the dynamic reserves and water invasion of water-invasion gas reservoirs using the principle of material balance equation [20]. Both the calculation of water invasion and dynamic reserves rely on the material balance equation [17–20]. It is challenging to simultaneously determine two dependent variables in the same equation, which makes it difficult to accurately calculate the influx index of water-invasion gas reservoirs. Moreover, previous studies often overlooked the influence of rock and bound water expansion and did not fully consider the compressibility of reservoir water and pores on the development of water-invasion gas reservoirs.

The Kela-2 gas field is currently the largest fully developed dry gas reservoir discovered in China, with a gas-bearing area of 48.1 square kilometers. It has geological reserves of natural gas totaling 2840.29×10^8 m^3, and a calculated recoverable reserve of 2130.22×10^8 m^3. The field exhibits several notable characteristics, including a high gas column height (448 m), a thick reservoir (550 m), high formation pressure (74.35 MPa), high pressure coefficient (2.022), and high well productivity. In the process of depletion during production, the reservoir pressure gradually decreases, leading to an increase in effective stress acting on rock particles. This effect can induce rock deformation, resulting in a reduction in rock properties, such as porosity, permeability, and pore compressibility, thereby affecting the dynamic flow of fluid in the gas reservoir and the productivity of

gas wells. These factors present numerous difficulties and challenges for efficient and rational development. Similar reservoirs with extremely high pressure coefficients like the Kela-2 gas field have not been previously discovered domestically, and research in this area remains largely unexplored. Although there are some gas fields abroad with pressure coefficients exceeding 2.0, they are generally smaller in scale and have not been extensively studied in this regard. The Kela-2 gas field has a large aquifer system, with aquifer factors ranging from 1 to 11 in different areas. The geological mechanical activities of fractures facilitate water intrusion, and the bottom and edge waters are almost simultaneously mobilized with the reservoir natural gas. The water influx rate per unit pressure difference is 50 m per year, resulting in a water influx volume of 168 million m^3 and a water influx volume per unit pressure drop of 4.5×10^6 m^3. The significant water influx causes a reduction in the gas storage pore volume of the reservoir, while the replenishment of water energy slows down the decrease in formation pressure. This driving mechanism is referred to as elastic water drive. After more than a decade of high-speed development, the Kela-2 gas field is facing challenges such as rapid water breakthrough in gas wells and non-uniform rise of gas/water interface. The invasion of bottom and edge waters has resulted in a decrease in the expected gas recovery rate from 85% to 67%. Calculating the water influx index at different stages of gas field development is of great significance for adjusting the development plan and improving natural gas recovery. The pore compressibility factor is an important parameter that affects the calculation of the influx index in gas reservoirs. Its value has a significant impact on water invasion and rock porosity expansion. Previous studies have suggested that under high-pressure conditions in reservoirs, the reservoir water compressibility factor remains relatively constant with pressure changes, but the pore compressibility factor exhibits noticeable variations [21,22]. Currently, there are three main methods for determining the pore compressibility factor: the empirical formula method, experimental measurement method, and theoretical calculation method. Since porosity is a more readily obtainable parameter, Hall conducted experiments on sandstone and limestone samples and established the relationship between the pore compressibility factor and porosity, creating the commonly used Hall chart [23]. However, the rock compressibility factor is a complex function of factors such as lithology, porosity, pore pressure, and cementation. The empirical formula method struggles to comprehensively consider the combined effects of multiple parameters [24]. The theoretical formulas require the determination of numerous parameters and involve making various assumptions for calculation convenience, thus not reflecting the real conditions of the reservoir rocks. Moreover, the calculation process is cumbersome and not conducive to practical production applications [25]. In comparison, an experimental measurement of the pore compressibility factor is the most accurate and effective approach. Currently, there are two main methods for pressure testing the pore compressibility factor: fixed pore fluid pressure with varying confining pressure and fixed confining pressure with varying pore fluid pressure [26,27]. In the development of gas reservoirs, the overburden pressure usually remains constant, while the pore pressure gradually decreases as development progresses, resulting in changes in effective stress. Therefore, the method of fixed confining pressure with varying pore fluid pressure is more capable of reflecting the actual pressure variations in reservoirs [28].

For water-invasion gas reservoirs, especially those with active water flooding, the calculation of dynamic geological reserves and water reservoirs is a crucial task. The first step in this process is determining the magnitude of water invasion, which poses a significant challenge. Numerous scholars, both domestically and internationally, have conducted extensive research on this topic, assuming various water invasion models and deriving calculation formulas for different types of water invasion. Li et al. established a material balance equation for water-invasion gas reservoirs considering the comprehensive compressibility factor of rock, which indirectly determines the water invasion using graphical methods [12]. Cai et al. developed a material balance calculation method considering water invasion for abnormal high-pressure gas reservoirs [29]. Sun et al. established a material balance equation for high-pressure gas reservoirs by considering the compressibility

factor of rock and assuming that the reserve and cumulative effective compressibility factor followed a power function relationship [14]. Zhu et al. improved the material balance equation for gas reservoirs by considering factors such as natural gas expansion, edge- and bottom-water invasion, rock expansion, and bound water expansion [13]. These existing methods for calculating the influx index can be referred to as the dynamic method when combined [13,14]. This method inversely calculates the driving index based on the known dynamic production data of gas wells. These methods have certain guiding significance for understanding the variation pattern of driving energy in gas reservoirs and adjusting development strategies accordingly. However, the dynamic method for calculating the influx index has several issues: (1) The pore compressibility coefficient is a key parameter that affects the calculation of the influx index, and its value affects the calculation of water invasion. However, testing the compressibility factor under high-pressure conditions in gas reservoirs is challenging. (2) The calculation of the influx index depends on the material balance equation and is greatly influenced by the dynamic reserve, which is a dynamic parameter that interacts with water invasion in the same equation, resulting in multiple solutions. In light of these issues, a static method is proposed for calculating the influx index. The static method calculates the influx index solely based on static parameters in the absence of known dynamic production data. However, the limitations of energy evaluation for water make it difficult to determine the water factor accurately, which significantly affects the results of the static method and makes it difficult to match the results with those of the dynamic method.

In 2001, the Kela-2 gas field was evaluated to have a proven geological reserve of 284 billion m^3 and a recoverable reserve of 213 billion m^3. In the first seven years of development until 2004, the average gas extraction rate remained around 4%. However, due to a lack of clear understanding of water energy during the initial stages of development and the geological mechanical activities of fractures facilitating water intrusion, after more than a decade of high-speed development, the Kela-2 gas field is facing challenges such as rapid water breakthrough in gas wells and non-uniform rise of the gas/water interface. Currently, the aquifer factor ranges from 4 to 5, and the gas extraction rate has been forced to adjust to 2.2%. It is crucial to understand the impact of water influx on the Kela-2 gas field. The water influx volume in the Kela-2 gas field gradually increases as the formation pressure decreases, and the rate of increase becomes larger. Currently, with the pressure in the Kela-2 gas field dropping to 33.6 MPa, the cumulative water influx volume is 182 million m^3, and the predicted water influx volume upon abandonment is 223 million m^3. The rate of water influx growth differs between the late development phase and the pre-development phase of the Kela-2 gas field. In the late development phase, water drive intensifies, and the rate of water influx growth accelerates. The water influx volume per unit pressure drops, increasing from 3 million m^3 in the pre-development phase to 8 million m^3 in the late development phase. The water influx volume per billion cubic meters of gas produced increases from 100,000 m^3 in the pre-development phase to 200,000 m^3 in the late development phase. In the late development phase of the Kela-2 gas field, intensified water influx becomes imperative for effective gas drainage. The original hydrocarbon pore volume of the Kela-2 gas field is 609 million m^3, and the original pore volume is 896 million m^3. Currently, with the formation pressure in the Kela-2 gas field decreasing to 33.6 MPa, the water invasion impact coefficient is 75%, and the water-invaded volume is 607 million m^3.

In this study, we established a testing method for the pore compressibility factor under reservoir conditions. By using kerosene as the experimental medium, maintaining a constant confining pressure, establishing an initial high pore fluid pressure state, and conducting controlled flow rate extraction to simulate reservoir development, we effectively eliminated the influence of kerosene compressibility on the calculation of the pore compressibility factor. This experiment successfully evaluated the compressibility of abnormally high-pressure water-invasion gas reservoirs and provided valuable guidance for accurately calculating the influx index. Furthermore, a combined iterative method was

developed to calculate the influx index, which compares the results obtained from the static and dynamic methods, dynamically adjusts the values of the dynamic reserve and water factor, iteratively corrects the pore compressibility factor using a binary search method, and conducts multiple iterations until the results of the static and dynamic methods are consistent. This approach enhances the reliability of influx index evaluation in water-invasion gas reservoirs. The proposed method is of great significance for controlling water invasion and maintaining stable gas production in water-invasion gas reservoirs.

2. Geological Settings

The Kuqa Depression is located on the northern edge of the Tarim Basin, adjacent to the Tianshan fold belt. It extends from the Wushen Depression in the west to the Yangxia Depression in the east, and is bordered by the southern Tianshan orogenic belt to the north and the Tabei Uplift in the south. The development and evolution of the basin are closely related to the Tianshan orogenic belt and the Tabei Uplift on both sides. Based on the current structural characteristics of the basin, the Kuqa Depression can be divided into the northern monocline belt, Wushen Depression, Kelasu thrust zone, Yiqikeli thrust zone, Baicheng Depression, Yangxia Depression, Qiulitag thrust zone, and southern slope belt. Among them, the Kelasu thrust zone, Yiqikeli thrust zone, and Qiulitag thrust zone are the most favorable areas for oil and gas accumulation. The discovered large gas fields such as Da Bei, Kelasu 2, and Dina 2 are all located in these structural units. Drilling and seismic data reveal that the sedimentary strata in the Kuqa foreland basin include the Triassic, Jurassic, Cretaceous, Paleogene, and Neogene from the bottom to the top. The main source rocks are lacustrine mudstones and coal-bearing formations of the Triassic–Jurassic Lake and swamp facies. The reservoirs are well developed and include the T1oh of the Lower Triassic Eohobrak Formation; the T2k of the Middle-Lower Triassic Kelamayi Formation; the J1y and J1a of the Lower Jurassic Yangxia and Ahe Formations; the J2k of the Middle Jurassic Kuzilienur Formation; the K1bx and K1bs of the Lower Cretaceous Bashikeqi and Baxigai Formations; the E1-2km of the Paleogene Kumugelimu Formation; the E2-3s of the Suweiyi Group; and the N1j and N1k of the Neogene Jidike and Kangcun Formations. The cap rocks mainly consist of gypsum, anhydrite, and salt rocks of the Paleogene Kumugelimu Formation and Jidike Formation. The Kelasu 2 gas reservoir is located in the Kelasu straight back fold of the Kuqa Depression, with the Lower Cretaceous Bashikeqi and Paleogene Kumugelimu Formation sandstones as the main gas-bearing layers. The cap rock is the salt rock of the Kumugelimu Formation, which is tight and has abnormally high pressure, indicating strong sealing capacity. The porosity and permeability of sandstone reservoirs are key factors controlling oil and gas production. In the Kelasu 2 gas field, the Upper Bashikeqi Formation of the Cretaceous and the Lower Kumugelimu Group of the Paleogene are the main natural gas reservoirs. The relationship between the measured porosity and permeability of the sandstone reservoirs in Well KL2-13 shows that the sandstone reservoirs in the Kelasu 2 gas field have relatively high porosity, with the highest values reaching 22.4% for porosity and 1770 mD for permeability. The porosity and permeability ranges of the Bashikeqi Formation and Kumugelimu Group sandstone reservoirs in Well KL2-13 are 4% to 20% and 0.02 mD to 551 mD, respectively, with average values of 11.3% for porosity and 34.5 mD for permeability. The porosity and permeability ranges of the Bashikeqi Formation and Kumugelimu Group sandstone reservoirs in Well Kelasu 201 are 1% to 22.4% and 0.01 mD to 1770 mD, respectively, with average values of 13.1% for porosity and 56.1 mD for permeability.

Due to the high initial production rate, the reservoir exhibited active water drive and strong energy, resulting in water breakthrough occurring much earlier than the design anticipated. The designed water breakthrough time was projected to be in 2025, with a 21-year water-free gas production period. However, water breakthrough was observed in 2008, leading to a significantly shortened water-free gas production period of only 3.3 years. Currently, 10 wells are producing water, with a water-to-gas ratio of 0.1811 tons per ten thousand cubic meters. After implementing protective development measures, the

decline rate of reservoir pressure slowed down, and the gas production per unit pressure drop gradually exceeded the design expectations. The Kela-2 gas field experienced rapid initial production rates, resulting in a fast decline in reservoir pressure. In recent years, the decline rate has slowed down, and the gas production per unit pressure drop has gradually increased (Figure 1). Currently, the reservoir pressure is 38.64 MPa, with a total pressure drop of 35.71 MPa and an annual pressure decline of 1.52 MPa. The pressure maintenance level is estimated to be 52.0%. After reducing gas production scale in 2011, the gas production per unit pressure drop gradually increased, reaching 40.71 billion m^3 per MPa in 2019.

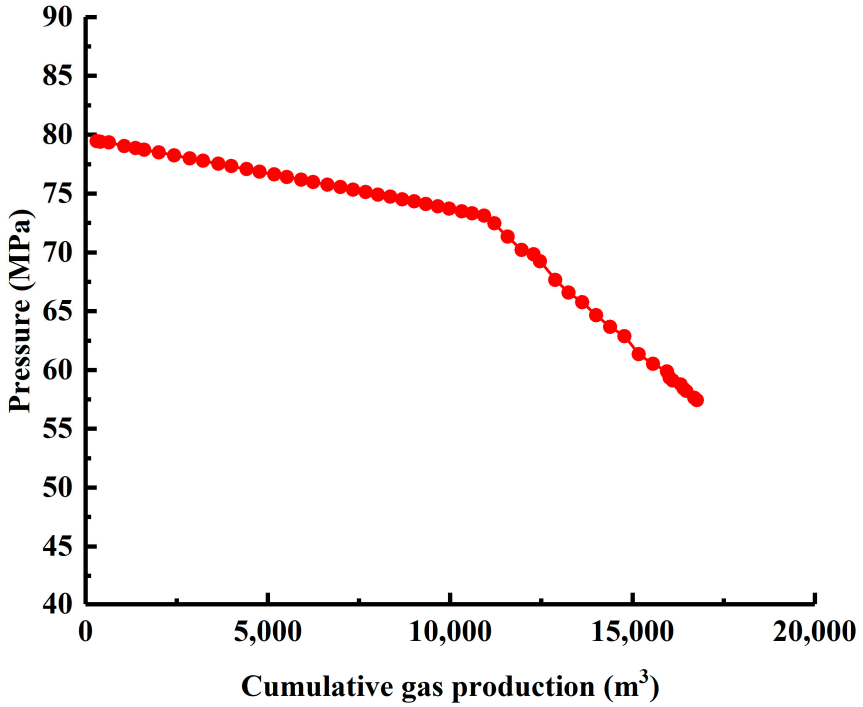

Figure 1. Relationship between the pressure and the cumulative gas production Kela-2 gas field.

3. Materials and Methodology

3.1. Materials

The core samples used in this experiment were obtained from the KL2-13 well in the Kela-2 reservoir. Its diameter, length, porosity, permeability, pore volume are 10.1 cm, 10.69 cm, 10.6%, 11.55 mD, and 10.6%, respectively.

3.2. Experimental Procedure and Methods

The experimental apparatus can be find in the Appendix A. The method involved saturating full-diameter core samples with kerosene, maintaining a fixed confining pressure, and varying the pore fluid pressure. The use of full-diameter core samples with large pore volumes reduced the impact of dead volume in the experimental procedure on the test results. Kerosene, compared to formation water, has lower sensitivity and therefore has a smaller impact on the calculation of the pore compressibility factor. The pressure changes during the experiment were consistent with the pressure variations in a reservoir development process, where the overburden pressure remains constant while the pore fluid pressure gradually decreases (Figure 2). This experimental setup closely mimicked the actual pressure changes in a reservoir during development, allowing the test results to better reflect the pore compressibility behavior during reservoir development (Figure 2).

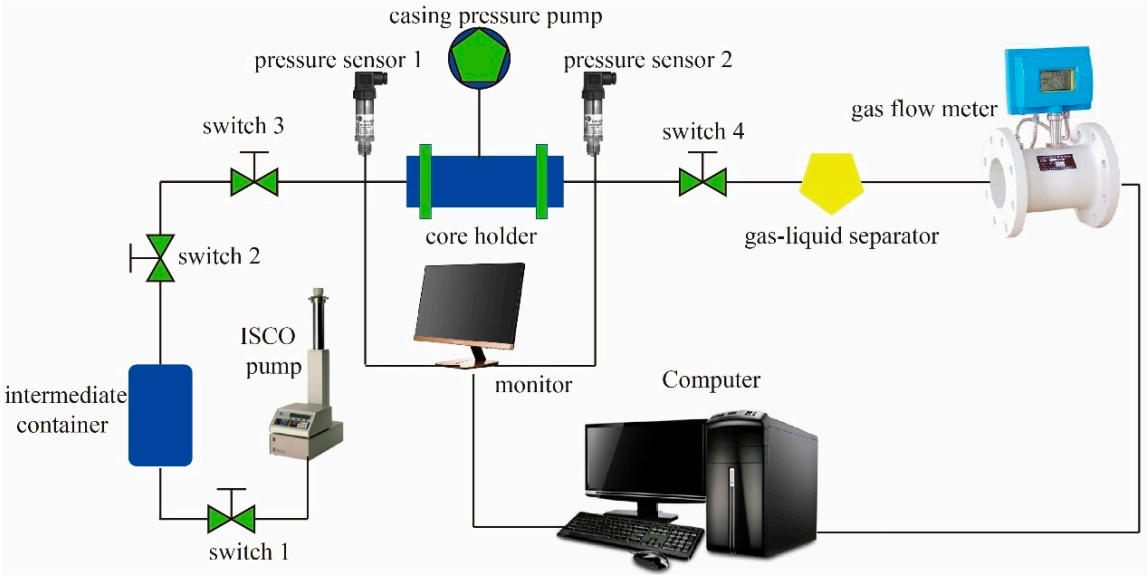

Figure 2. Experimental flowchart for testing the pore compressibility factor under reservoir conditions.

Due to the high formation pressure of the Kela-2 gas reservoir, the working pressure of the core holder and intermediate container used in the experiment was set at 50 MPa. In order to closely simulate the formation conditions, it was necessary to approximate the experimental pressure to the actual formation pressure. The effective stress was determined using the following equation [30]:

$$P_e = P_{gf} - P \tag{5}$$

$$P_{gf} = \rho h/100 \tag{6}$$

where P_e represents the effective pressure, in MPa; P_{gf} denotes the overburden pressure, MPa; P refers to the formation fluid pressure, in MPa; ρ represents the density of the overburden rock, g/cm^3; and h represents the thickness of the overburden reservoir, m.

The average density of the overburden rocks in the Kela-2 gas field was taken as 2.36 g/cm^3. The thickness of the overburden was assumed to be 3750 m, which corresponds to the middle depth of the gas reservoir. Based on these values, the overburden pressure was calculated to be 88.50 MPa and the formation fluid pressure to be 74.35 MPa. Consequently, the initial effective stress could be determined as 14.15 MPa. From Table 1, it can be observed that the pressure under laboratory conditions is two-thirds of the pressure under reservoir conditions.

Table 1. Approximation of laboratory pressure to reservoir pressure conditions.

Reservoir Condition		**Laboratory Approximate Conditions**	
overburden cap rock pressure	88.5 MPa	confining pressure	59 MPa
reservoir fluid pressure	74.35 MPa	pore fluid pressure	50 MPa
effective pressure	14.15 MPa	effective pressure	9 MPa

The specific experimental procedure is outlined as follows: (1) Full-diameter rock cores were vacuum saturated with kerosene (density of 0.8 g/cm^3) to eliminate the influence of water sensitivity. (2) The cores were then pressurized and saturated to establish an initial high-pressure flow state. (3) Controlled flow rate extraction was performed to simulate reservoir development, during which pore fluid pressure and outlet liquid volume were recorded. (4) The comprehensive pore compressibility factor (including both pore compressibility and kerosene compressibility) was calculated based on the pore fluid pressure, liquid volume, and core pore volume. (5) Kerosene was injected into a rigid

container filled with kerosene using an ISCO pump, and the kerosene compressibility factor was determined by analyzing the pressure variations inside the container and the injected liquid volume. (6) The influence of kerosene compressibility on the experiment was eliminated, and the pore compressibility factor was calculated.

$$C_{fe} = \frac{\Delta m_k}{\rho_k} \frac{1}{V_p \Delta p} \tag{7}$$

where C_{fe} represents the experimentally measured comprehensive pore compressibility factor, MPa^{-1}; Δm_k denotes the kerosene oil production, g; ρ_k represents the density of kerosene, g/cm^3; V_p represents the pore volume of the rock core, cm^3; and p represents the pore pressure, MPa.

$$C_{\mathrm{fk}} = \frac{V_s - V_o}{\Delta p} \tag{8}$$

where C_{fk} represents the compressibility factor of kerosene, MPa^{-1}; V_s denotes the initial pumped liquid volume, mL; V_o represents the final pumped liquid volume, mL; Δp represents the pressure difference before and after the rigid container experiment, MPa.

$$C_f = C_{fe} - C_{fk} \tag{9}$$

where C_f represents the pore compressibility factor, MPa^{-1}.

Equation (9) represents the calculation formula for the pore compressibility factor in this experiment.

4. Results and Discussion

During the experimental process, the flow rate data were recorded every time the pore fluid pressure decreased by 5 MPa, with a kerosene production of approximately 0.7 g. The pore compressibility was calculated based on kerosene density, and the comprehensive pore compressibility factor was determined using the definition formula for the pore compressibility factor. The results showed that the comprehensive pore compressibility factor was not significantly influenced by pressure and remained relatively constant. To eliminate the influence of kerosene compressibility on the calculation of the pore compressibility factor, kerosene was injected into a 1000 mL intermediate container filled with kerosene using an ISCO pump until the pressure reached 50 MPa. This allowed us to observe the variation of the kerosene compressibility factor with pressure.

Kerosene, as the medium used in the experiment, exhibits a gradual decrease in its compressibility coefficient with increasing pressure, with a relatively small variation range (Table 2). The actual pore compressibility coefficient is equal to the comprehensive pore compressibility coefficient minus the kerosene compressibility coefficient, ranging from 0.00075 to 0.00096/MPa (Figure 3). As there is no medium that is completely incompressible, the actual pore compressibility coefficient should be similarly influenced to a small extent by pressure, remaining relatively constant at approximately 0.00085/MPa (Figure 3, Table 3).

Table 2. Pore compressibility factor test results for core sample 4-13/29 of KL2-J3 well.

Number	Pore Fluid Pressure (MPa)	Pore Fluid Pressure after the Experiment (MPa)	Stage Pressure Drop (MPa)	Fluid Pressure (MPa)	Oil Production (g)	Pore Compressibility (mL)	Pore Compressibility Factor (1/MPa)
1	49.97	45.01	4.96	47.49	0.688	0.86	0.00174
2	45.01	39.98	5.03	42.49	0.712	0.89	0.00177
3	39.98	35.03	4.95	37.50	0.717	0.90	0.00181
4	35.02	30.01	5.01	32.51	0.71	0.89	0.00177
5	30.01	24.99	5.02	27.50	0.715	0.89	0.00178
6	24.99	20.01	4.98	22.50	0.724	0.91	0.00182

Table 2. *Cont.*

Number	Pore Fluid Pressure (MPa)	Pore Fluid Pressure after the Experiment (MPa)	Stage Pressure Drop (MPa)	Fluid Pressure (MPa)	Oil Production (g)	Pore Compressibility (mL)	Pore Compressibility Factor (1/MPa)
7	20.02	15.01	4.99	17.50	0.718	0.90	0.00180
8	15.04	10.01	5.04	12.52	0.709	0.89	0.00176
9	10.02	5.04	4.98	7.53	0.703	0.88	0.00177
10	5.01	2.52	2.49	3.765	0.354	0.44	0.00177

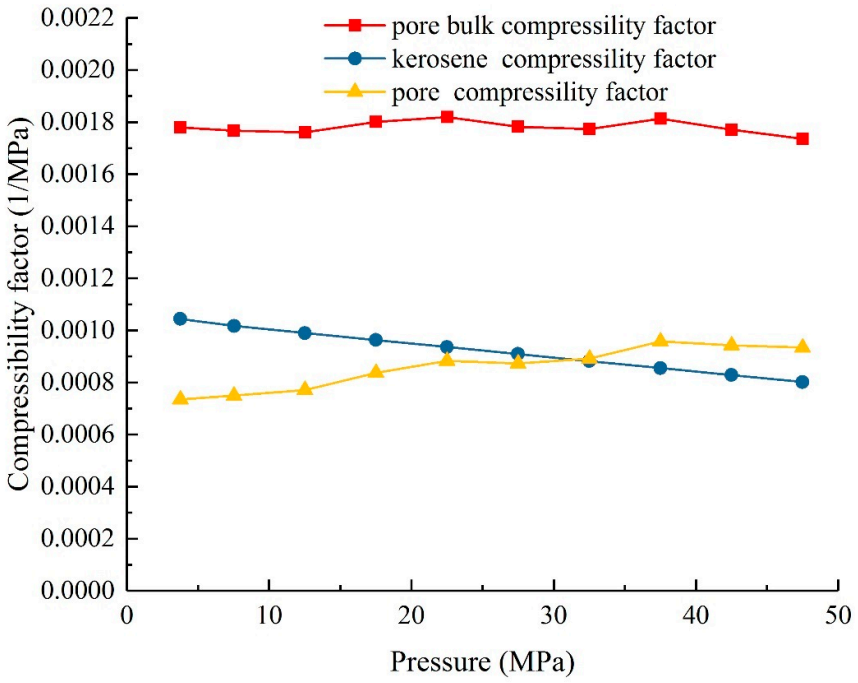

Figure 3. Test results of pore compressibility factor under reservoir conditions.

Table 3. Kerosene compressibility coefficient test results.

Pressure in Intermediate Container (MPa)	Initial Pump Volume (mL)	Final Pump Volume (mL)	Liquid Volume Difference (mL)	Compressibility Factor of Kerosene (1/MPa)
5	168.43	158.29	10.14	0.002028
10	158.29	153.17	5.12	0.001024
15	153.17	148.13	5.04	0.001008
20	148.13	143.23	4.9	0.00098
25	143.23	138.47	4.76	0.000952
30	138.47	133.87	4.6	0.00092
35	133.87	129.38	4.49	0.000898
40	129.38	125.07	4.31	0.000862
45	125.07	120.83	4.24	0.000848
50	120.83	116.77	4.06	0.000812

4.1. New Method for Calculating Influx Index

The existing method for calculating the influx index is known as the dynamic method, which utilizes known dynamic production data from gas wells to calculate the influx index using Equation (1). The influx index obtained from the dynamic method is referred to as $WEDI_2$. In contrast, the new method is designed to calculate the influx index in situations where the dynamic production data from gas wells are unknown. It relies on static parameters, such as G, β, C_f, C_w, and the material balance equation to calculate the cumulative water invasion, cumulative gas production, and cumulative water production at different reservoir pressures. The influx index is then determined based on these calculations.

The size of a water body in a gas reservoir is usually measured by the ratio of the volume of the water body to the volume of the gas reservoir, i.e., a water body multiple. The water body multiple is obtained by measuring the size of the sand body with tectonic maps in relation to the geological aspect. Moreover, it is also fitted by the production data with regard to the developmental aspect. The water body multiple can be calculated with the following formula:

$$\beta = \frac{V_w}{V_o} \tag{10}$$

where β is the water body multiple; V_w is the water body volume, m^3; V_o is the gas reservoir volume, m^3.

Firstly, the water invasion is calculated using the formula method based on the water body multiple and compressibility factors. The calculation formula is as follows [31]:

$$W_e = \beta G B_{gi} \int_P^{P_i} \frac{C_w + C_{f1}}{S_{wi}} dp \tag{11}$$

According to the material balance equation, the cumulative gas production and cumulative water production volumes are calculated under reservoir conditions. The calculation formula used for this is Equation (2).

Since, in general, the difference between water production and gas production is orders of magnitude apart, particularly in the early stages of gas field development, the cumulative gas production can be calculated using the following formula [32]:

$$G_p = G - \frac{GB_{gi}}{B_g} - \frac{\Delta V_w + \Delta V_r}{B_g} + \frac{W_e}{B_g} \tag{12}$$

By substituting Equations (8) and (9) into the definition Formula (1) for the influx index, we obtain [33] the following:

$$WEDI_1 = \frac{\beta G B_{gi} \int_P^{P_i} (C_w + C_{f1}) dp}{G(B_g - B_{gi}) - \Delta V_w - \Delta V_r + \beta G B_{gi} \int_P^{P_i} (C_w + C_{f1}) dp} \tag{13}$$

Equation (11) represents the proposed method for calculating the influx index, referred to as the static method. The static method can predict variations in the reservoir invasion index based on the geological characteristics of the reservoir before gas field development. However, obtaining accurate energy parameters for water in the early stages of development is challenging, often resulting in a range of values. Additionally, the invasion of water has a significant impact on dynamic reserves, introducing uncertainties. The existing calculation method for the influx index is called the dynamic method, which utilizes the known dynamic development data of gas wells during the production process to calculate the influx index. In the process of calculating the influx index, the pore compressibility coefficient (C_f) is considered as a function. Therefore, a new method that combines both static and dynamic approaches is proposed to calculate the influx index.

The existing calculation method for the influx index is called the dynamic method, which utilizes the known dynamic development data of gas wells during the production process to calculate the influx index. In the process of calculating the influx index, the pore compressibility coefficient (C_f) is considered as a function. The static method can predict the changes in the reservoir drive index based on the geological characteristics of the reservoir before its development. However, obtaining accurate parameters for water properties is difficult in the early stages of development, and, usually, only a certain range can be provided. The intrusion of water has a significant impact on dynamic reserves, introducing uncertainty. Therefore, it is challenging to accurately determine the static parameters.

The specific calculation process is illustrated in Figure 4. The calculation steps are as follows: (1) Known parameters include G, C_{f1}, β, original reservoir pressure, gas production rate, and formation pressure. (2) The static method calculates the $WEDI_1$. (3) The dynamic

method calculates the $WEDI_2$ and uses the calculated water invasion to estimate the C_{f2}. (4) If $WEDI_1$ matches $WEDI_2$ and C_{f2} matches C_{f1}, the calculation results are considered reliable, and the calculation process is completed. Otherwise, based on the differences between the two methods' influx indexes, the values of the G and the β are adjusted, and the C_{f1} is revised using the bisection method as $C_{f1} = 0.5 \times (C_{f1} + C_{f2})$. This process continues until $WEDI_1$ matches $WEDI_2$ and C_{f2} matches C_{f1}, indicating the completion of the influx index calculation [34].

$$C_{f2} = \frac{G_p B_g + W_p B_w - G(B_g - B_{gi}) - \Delta V_w - \Delta V_r}{\beta G B_{gi\Delta p}} - C_w \quad (14)$$

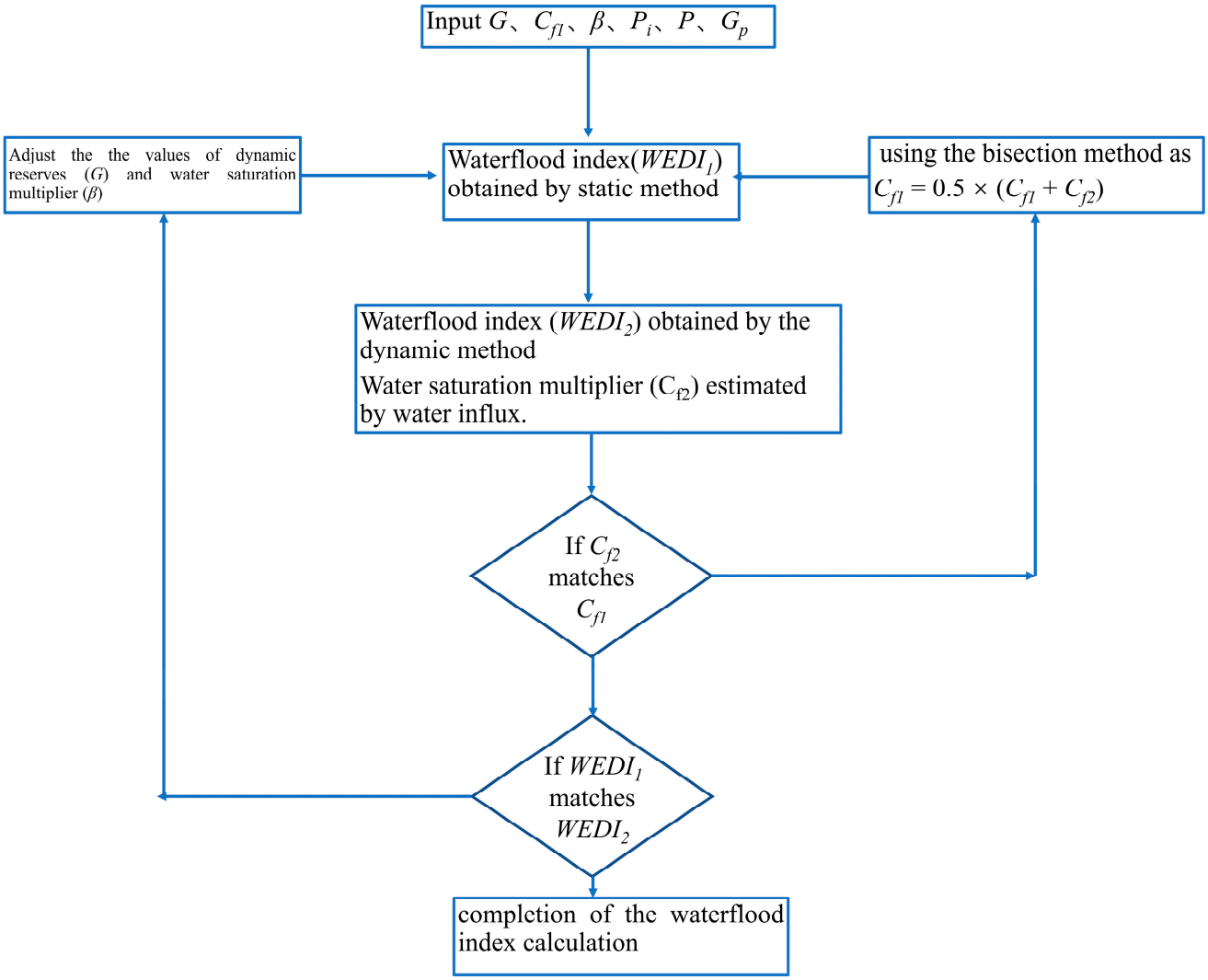

Figure 4. Flowchart of the iterative method combining static and dynamic approaches for calculating the influx index.

4.2. Application and Analysis of Influx Index Calculation in Water-Invasion Gas Reservoirs

In the Kela-2 gas field, the evaluated geological reserves were 284 billion m^3 with recoverable reserves of 213 billion m^3 in 2001. During the first seven years of development starting from 2004, the average gas production rate was maintained at around 4%. However, due to a lack of clear understanding of water energy in the early stages of development and favorable geological mechanical activities for water invasion in the fractured reservoir, the Kela-2 gas field has faced challenges such as rapid water breakthrough in gas wells and non-uniform rise of the gas/water interface after over a decade of high-speed development.

Currently, a water body multiple of 4 to 5 is being used, and the gas production rate has been forced to be adjusted to 2.2%. It is crucial to understand the impact of water invasion on the Kela-2 gas field. The pore compressibility factor obtained from constant confining pressure variable pore fluid pressure experiments was used to calculate the influx index. Due to the significant difference between the evaluated reserves and recoverable reserves, the dynamic method was used to calculate the influx index curves for dynamic reserves of 284, 240, and 200 billion m^3, while the static method was used to calculate the influx index curves for water body multiples of 4, 4.5, and 5.

From the comparison between the results obtained by the dynamic and static methods, it can be observed that the dynamic method is less influenced by pressure, while the static method shows a significant decrease in the influx index as the pressure decreases (Figure 5). In the Kela-2 gas field, the dynamic reserves ranging from 200 to 240 billion m^3 coincide more with the results obtained with the static method. Through an extensive analysis of production data, the dynamic reserves were adjusted to 235 billion m^3, and the water body multiple was set to 4.8 for the iterative fitting of the influx index curve.

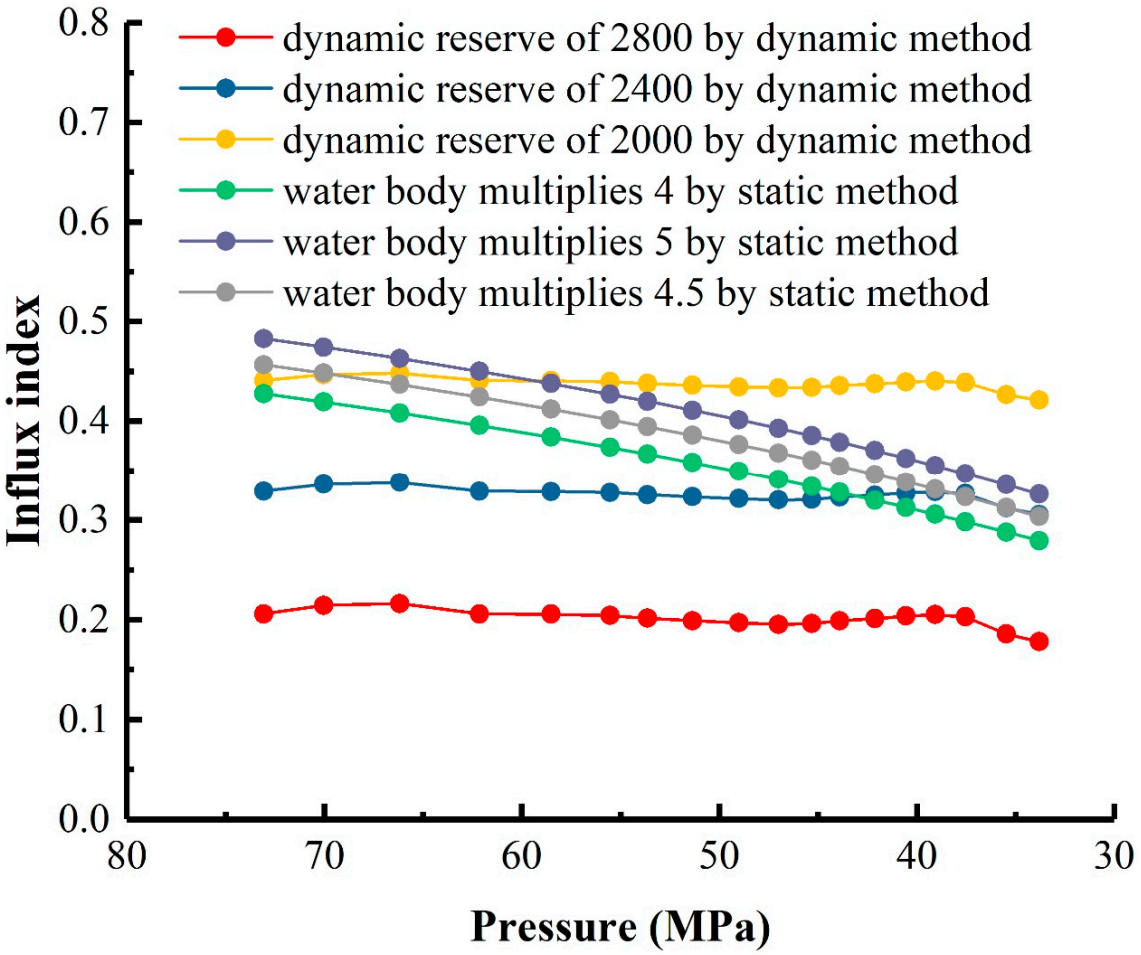

Figure 5. Water invasion index result of the Kela-2 gas field obtained with the dynamic method and the static method.

The discrepancy between the results obtained with the dynamic and static methods can be attributed to the issue of pore compressibility factor (C_f) values (Figures 6 and 7). The pore compressibility factor C_{f1} used in the static method and the pore compressibility factor C_{f2} calculated dynamically only fit well under low-pressure conditions (Figures 6 and 7). Therefore, a bisection method was employed to revise C_{f1} and perform iterative calculations.

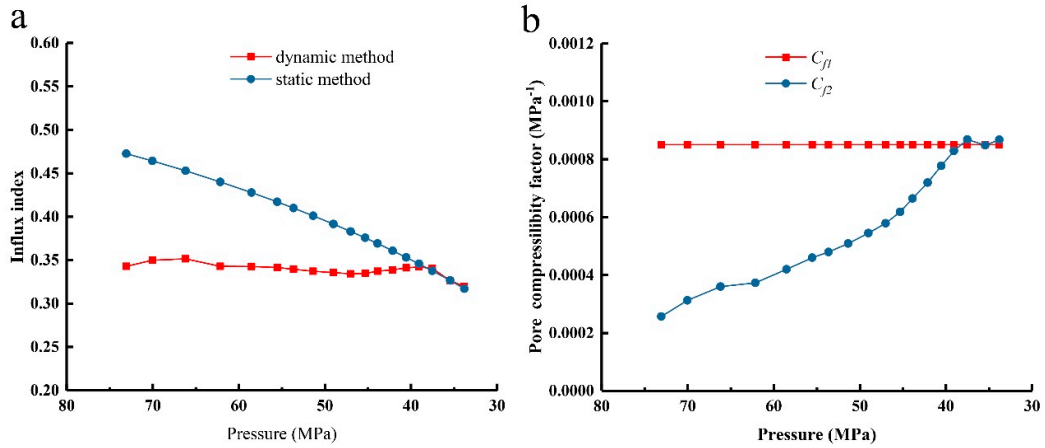

Figure 6. The calculation results of water invasion index and pore compressibility factor. (**a**) Water invasion indices using the dynamic method and the static method. (**b**) Comparison result of the adopted pore compressibility factor with the dynamically calculated pore compressibility factor.

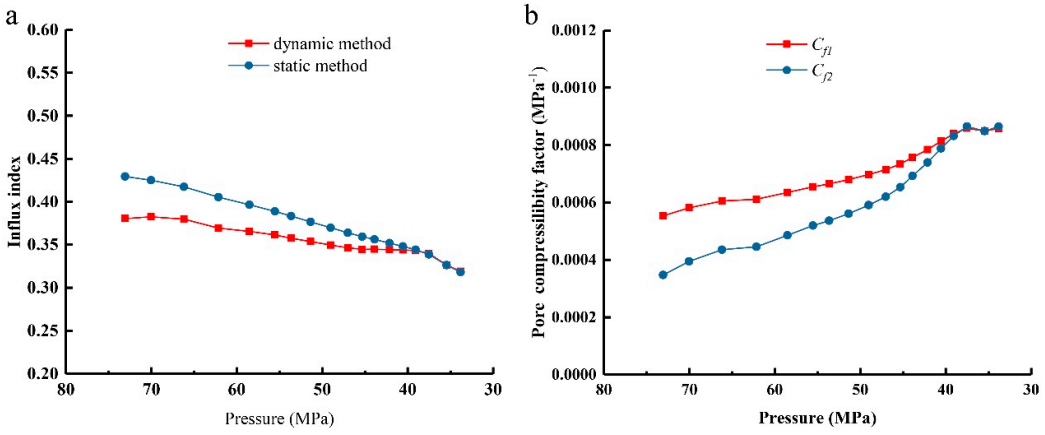

Figure 7. The calculation results of water invasion index and pore compressibility factor after one iteration. (**a**) Calculation results of water invasion index after one iteration. (**b**) Comparison result of pore compressibility factors after one iteration.

Through multiple iterations, the influx index calculation results obtained with the static and dynamic methods exhibit an increasing level of fit, eventually achieving a good fit (Figures 8 and 9). The real pore compressibility factor curve of the gas reservoir is obtained, as shown in Figure 9b. The difference between this curve and the pore compressibility curve obtained from constant confining pressure variable porosity fluid pressure experiments is minimal, especially in the low-pressure range. The pore compressibility factor is not significantly influenced by pressure. From the unit pseudo-pressure production degree curve of the Kela-2 gas field (Figure 10a), it can be observed that the gas production degree is 8.4 billion m^3 when the pseudo-pressure is greater than 43 MPa (pressure of 55 MPa), and 7.7 billion m^3 when the pseudo-pressure is below 43 MPa. The difference between the two values is 8.3%, which is relatively small. Therefore, the difference in the static pore compressibility factor is also small and consistent with the results reflected by the pore compressibility factor curve.

Furthermore, according to the definition of the displacement index, a combined static/dynamic iterative method was used to establish the displacement index chart for the Kela-2 gas field. In this chart, the gas displacement index represents the percentage of natural gas driving energy in the total driving energy [35].

$$I_1 = \frac{G(B_g - B_{gi})}{G_p B_g + W_p B_w} \tag{15}$$

where I_1 is defined as the gas displacement index, and is dimensionless.

The rock and connate water displacement index represent the percentage of energy contributed by rock pore compressibility and formation water expansion in the total driving energy [36,37].

$$I_2 = \frac{\Delta V_w + \Delta V_r}{G_p B_g + W_p B_w} \tag{16}$$

where I_2 is defined as the rock and connate water displacement index, and is dimensionless.

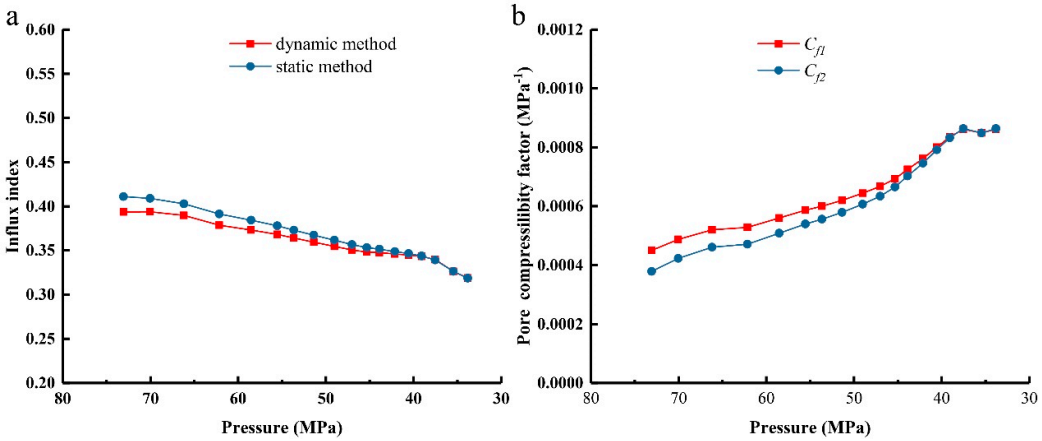

Figure 8. The calculation results of water invasion index and pore compressibility factor after two iterations. (**a**) Calculation results of water invasion index after two iterations. (**b**) Comparison result of pore compressibility factors after two iterations.

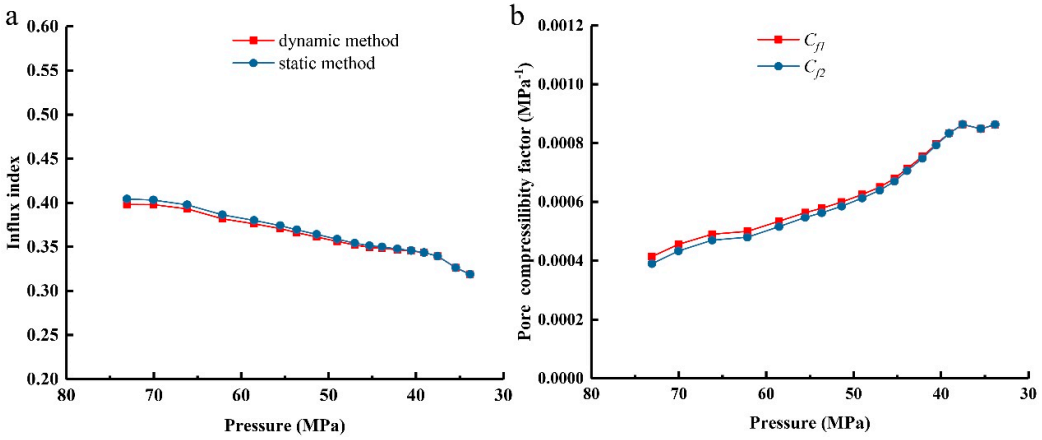

Figure 9. The calculation results of influx index and pore compressibility factor after three iterations. (**a**) Calculation results of water invasion index after three iterations. (**b**) Comparison result of pore compressibility factors after three iterations.

Through the combined static/dynamic iterative method, a well-fitted displacement index curve for the Kela-2 gas field was obtained (Figure 10b). The dynamic reserves were adjusted to 235 billion cubic meters, with a water body multiple of 4.8. The displacement indices calculated with the dynamic and static methods were consistent, and the gas production per unit pressure drop matched the actual production, indicating reliable evaluation results. The gas displacement index gradually increases with decreasing formation pressure, but the magnitude of change is not significant. Overall, it remains above 0.5, with an average of 0.55. The fundamental characteristic of water-invasion reservoir development is still the depletion of the reservoir's own elastic energy. The influx index gradually decreases with decreasing formation pressure, but the magnitude of change is not significant. Overall, it remains above 0.3, with an average of 0.35, indicating that the Kela-2 gas field belongs to the category of strong water-invasion reservoirs. The rock and connate water displacement

indices are not significantly influenced by pressure, with an average value of 0.1. This confirms that the pore compressibility factor and formation water compressibility factor are minimally affected by pressure.

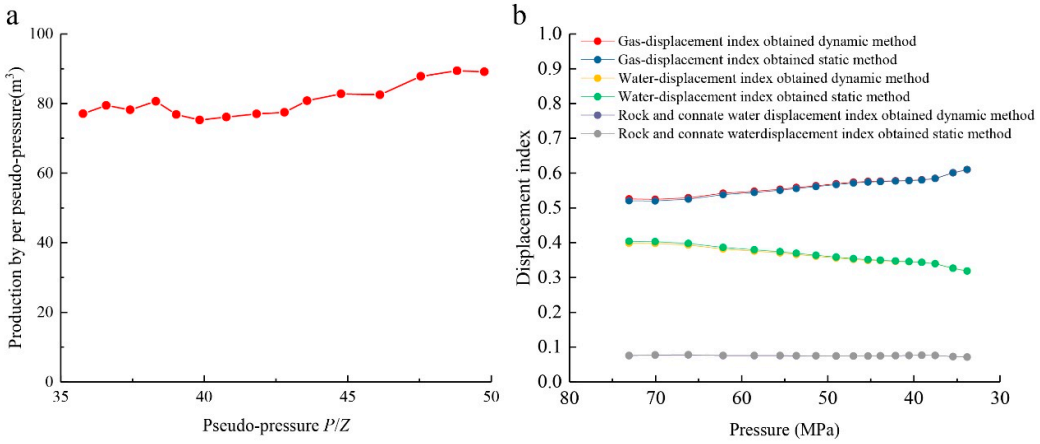

Figure 10. Production degree curve and displacement index of the Kela-2 gas field. (**a**) Pseudo-pressure production degree curve; (**b**) displacement index chart.

4.3. Comparison of the Influx Index Using Different Methods

In the field of water influx calculation, extensive research has been conducted by both domestic and foreign scholars. Among the most renowned calculation methods are the water influx models proposed by Van Everdingen, Hurst, and Fetkovich. However, these models are criticized for their overly idealized assumptions and complex calculations, limiting their practical applicability. Accurate application of these models requires a thorough understanding of the subsurface flow mechanisms and static parameters of the reservoir. Additionally, the complexity of the calculation process can result in significant deviations in the computed results. A comparative analysis is conducted to evaluate the performance of the Van Everdingen, Hurst, and Fetkovich models against a newly developed model (Figure 11). The comparative study reveals that while the Van Everdingen, Hurst, and Fetkovich models provide a sound theoretical framework for water influx calculation, their practical utility is limited. These methods require only production data and pressure measurements, making the calculation process relatively simple. They are widely applied in conventional gas reservoirs but have limitations when used in water-drive gas reservoirs.

The steady-state method is a water influx calculation approach used for water invasion models where the water influx rate does not vary with time. To achieve a stable flow, an external, extremely large natural water body with a sufficiently high permeability must exist outside the reservoir. In 1936, Schilthuis proposed the simplest steady-state model based on Darcy's law [9]. This model assumes that the water influx rate is directly proportional to the pressure drop in the formation. It assumes that the outer boundary pressure of the natural water body is a constant, equal to the original formation pressure. The flow behavior of the formation water follows Darcy's law, and the physical properties such as viscosity and permeability of the formation water remain constant. The integral representation of the model is expressed in a discrete form as follows [9]:

$$(We)_n = B\sum_{j=1}^{n}\left(p_i - \frac{p_{j-1}+p_j}{2}\right)(t_j - t_{j-1}) \quad (17)$$

where p_i is original formation pressure, MPa; P_j is reservoir pressure at any arbitrary time point; B is the water influx constant, m^3/d; and t_j is the reservoir production time, d.

In this model, the water influx rate remains constant without attenuation. However, this model does not consider the compressibility of the reservoir and the natural water body, leading to an overestimation of the calculated results. Nevertheless, this method is

simple and convenient, making it suitable as an approximate calculation method for initial estimations. Steady-state flow methods for water influx calculation are suitable for gas reservoirs with infinite aquifers or abundant water supply. However, in practical reservoir development, it is rare to encounter steady-state flow conditions for water invasion. Consequently, steady-state water influx models are not applicable to real-world scenarios.

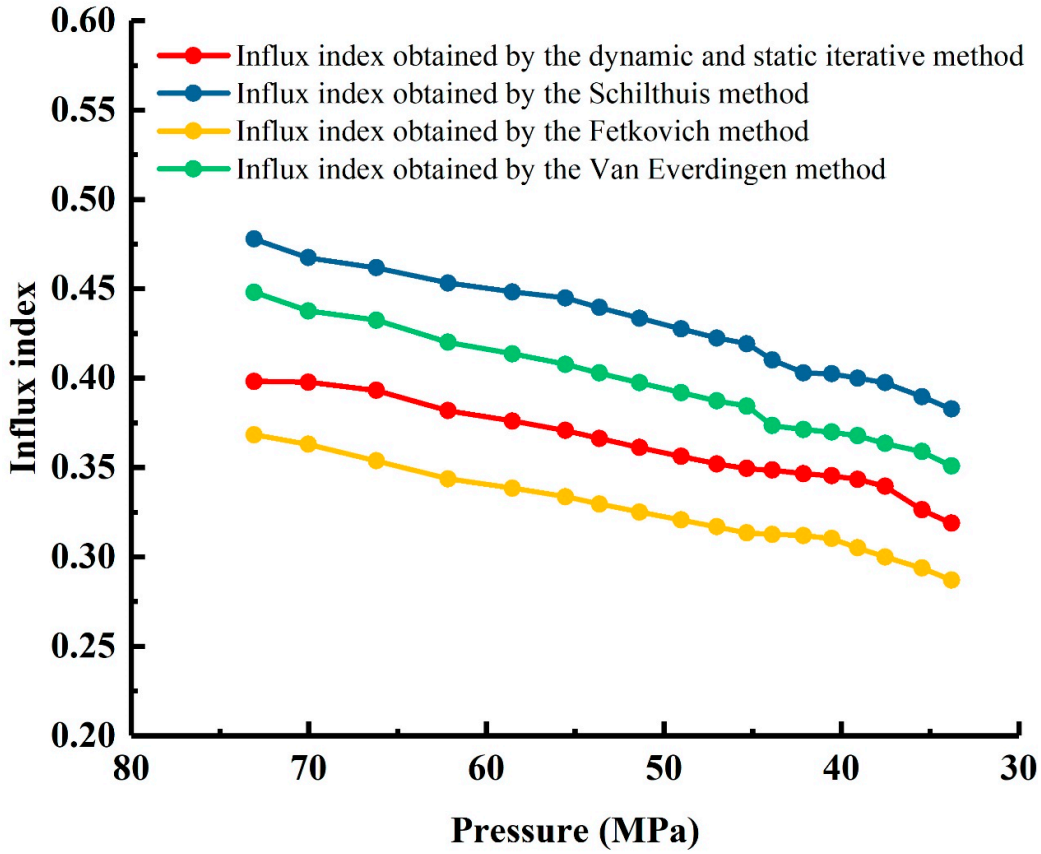

Figure 11. Comparison of influx index obtained using different methods.

In 1943, Hurst proposed an improvement to the water influx calculation equation of the Schilthuis steady-state model [10]. He suggested that during water invasion into oil and gas reservoirs, a portion of the flow exhibits transient behavior. This study investigates and discusses the modified water influx calculation equation proposed by Hurst as an enhancement to the Schilthuis model [10]. In 1949, A.F. Van Everdingen and W. Hurst introduced a widely used water influx calculation method known as the non-steady-state radial flow water influx model [10]. This model is applicable specifically to reservoirs exhibiting a planar radial or linear system in the water supply zone. The non-steady-state method refers to a water influx calculation approach for water invasion models in which the water influx rate varies with production time. This model considers the gas/water pressure at the boundary as a constant and assumes a homogeneous and uniform thickness reservoir. The mathematical formulation of this model is expressed as follows [10]:

$$W_e = B\Delta p Q_D\,(t_D, r_{eD}) \tag{18}$$

where Δp is the pressure drop across the water body, MPa; $Q_d\,(t_D)$ is the dimensionless water influx; t_D is the dimensionless production time.

In 1971, Fetkovich proposed a method for estimating water influx in gas reservoirs by considering the early stage unstable flow and utilizing a combination of pseudo-steady-state water influx index and material balance equations for the reservoir system [11]. This method treats the entire gas reservoir as a single well produced from the water supply

zone and derives a water influx calculation equation using flow equations. The Fetkovich method is applicable to reservoirs with both finite and infinite aquifer sizes [11]. For a finite and arbitrarily shaped natural water body, when the production time of the reservoir is sufficiently long, the aquifer reaches a pseudo-steady state. This model assumes that water influx is directly proportional to the pressure drop between the aquifer and the gas/water interface, neglecting the effects during non-steady-state periods, which may result in underestimated values. The mathematical formulation of the model is as follows [11]:

$$W_e = \frac{W_{ei}}{p_i}\ (p_i - p)\exp\ (-\frac{Jp_i t}{W_{ei}}) \tag{19}$$

where W_{ei} is the initial water that can be encroached in place at initial pressure p_i, m^3.

The influx index obtained with the Schilthuis method is the largest, and the error is also the largest (Figure 11). This is because the model assumes that the water invasion velocity is proportional to the pressure drop, where the pressure P is measured at the gas/water interface. The model assumes that the pressure at the outer edge of the water layer is constant and equal to the initial formation pressure P_i. The flow rate entering the reservoir is assumed to be proportional to the pressure difference (Darcy's law). The model also assumes constant viscosity of water, average permeability of the water layer, and geometric shape of the water layer. The model is rarely used to determine water invasion volume. The transient nature of the aquifer indicates that the water invasion volume is a function of time and reservoir pressure. In real gas reservoir development processes, permeability exhibits strong heterogeneity, and Darcy's law is not applicable. Also, due to the significant phenomenon of bottom water coning, it is difficult to maintain a constant geometric shape of the water layer. Therefore, the influx index obtained with this model has a larger error compared to other methods. In this model, the variation in production rate has an instantaneous impact on the water invasion from the water layer. The compressibility of the system is not considered here, which is not a realistic condition. However, this method is easy to use and can be considered as an approximate method at least for initial levels. In the non-steady-state model, the pressure in the water layer is not completely stable because the invading water undergoes continuously increasing distances. The Fetkovich method is applicable to finite water bodies, while the Van Everdingen method is applicable to infinite water bodies. Since the water body of the Kela-2 gas reservoir is relatively large, the results obtained with the Van Everdingen method are closer to the real level compared to the Fetkovich method (Figure 11). The predictions obtained using the Fetkovich method do not consider the water coning phenomenon during the production process. Therefore, the predicted values obtained with the Fetkovich method are slightly lower than those obtained using the Van Everdingen method (Figure 11).

To apply the dynamic and static iterative model, the assumption of constant pressure drop across the entire water layer needs to be modified using the superposition method to a series of constant pressure drops. The pressure dynamics are divided into several time intervals, and within each time interval, the average pressure can be considered constant. This approximation is satisfactory when the time intervals are very small. The constant pressure used within any given time interval is the average pressure between the start and end of the interval. The pressure difference used to calculate water invasion volume is related to the pressure in each time interval.

This study investigates commonly used methods for calculating the water influx, including the Schilthuis steady-state model, the Van Everdingen and Hurst unsteady-state model, and the Fetkovich pseudo-steady-state model. The Schilthuis and Fetkovich models simulate a water influx in limited aquifers using the Darcy flow equation and water-cut index, respectively, without considering gas reservoir types and water distribution characteristics. The Van Everdingen and Hurst method considers a non-steady-state water influx involving radial and linear flows, enabling an accurate prediction of water influx dynamics in edge-water gas reservoirs. However, it exhibits deviations in predicting water influx dynamics and aquifer storage in bottom-water gas reservoirs. Traditional dynamic

reserve calculation methods for water-driven gas reservoirs often overlook the impact of an external water influx or are limited to scenarios where the water influx calculation model is already known. These methods also require knowledge of water influx magnitude and long-term shut-in test pressure or continuous production test data. As a result, these methods face significant limitations when applied in practical scenarios. The newly developed model, on the other hand, demonstrates superior performance in terms of accuracy and simplicity (Figure 11). The results highlight the need for a more practical approach in water influx calculations.

4.4. Factors Affecting Water Invasion in Kela-2 Gas Field

Permeability, non-Darcy flow coefficient, and relative permeability (co-current three-phase area) are important factors that reflect the characteristics of reservoir and fluid flow in gas reservoirs. There is a certain correlation between these factors. On the other hand, effective thickness, gas supply boundary, and water invasion rate are macroscopic parameters that reflect the properties of the reservoir and water, but they are not the determining factors of reservoir fluid flow. Permeability has the most significant impact on the dynamic water invasion in edge-water gas reservoirs. When permeability changes, both the non-Darcy flow coefficient and relative permeability will also change. Generally, the larger the permeability, the faster the advancement of edge water, and the stronger the heterogeneity, resulting in a more pronounced non-piston displacement characteristic of edge water and lower recovery efficiency. Although the water invasion rate is not directly related to the dynamic water invasion, maintaining a reasonable reservoir pressure can reduce the water invasion rate, promote a uniform waterfront advancement, and reduce local gas enrichment, thereby improving the ultimate recovery efficiency of the water-drive gas reservoir. Therefore, from a production perspective, establishing a reasonable gas production intensity (or gas well operation system) is an important means to control the water invasion rate and maintain stable water levels. The key to water control production in gas wells lies in controlling the production pressure difference, with the focus on early identification and control of water invasion in gas reservoirs. Therefore, based on the study of the timing, effectiveness, and optimal drainage volume of reservoir drainage, differentiated water control strategies should be formulated according to different water invasion conditions in different regions to ensure that the scientific and efficient development of gas reservoirs continues to grow.

Production wells exhibit different water production characteristics controlled by various geological factors and manifest different water invasion patterns under the main controlling factors. The differentiated water production characteristics of production wells reflect the distribution characteristics of different reservoir properties. In the case of strongly heterogeneous bottom-water sandstone gas reservoirs, water easily invades the bottom of the well along the fracture network or high-permeability streaks. The rapid increase in the water/gas ratio reflects strong reservoir heterogeneity, while a slow or stable increase in the water/gas ratio indicates good reservoir homogeneity. In addition, structural factors, beach connectivity, water saturation and distribution, trapped gas in water, pore compressibility, and production systems are also important factors that affect the strength of water invasion.

The Kela-2 gas field has highly developed fractures, and the production wells are typically classified into two types: stable water production wells and composite water production wells. Stable water production wells have relatively undeveloped fractures and high-permeability layers, but a uniform distribution of fine network fractures forms a homogeneous reservoir with dissolution pores. Formation water slowly invades the interior of the gas reservoir, resulting in a finger-like, advance pattern of edge water. Composite water production wells are located in the gas/water transition zone, closer to the edge water, with a water layer in the lower part of the reservoir. In the early stage of development, bottom water easily breaks through the bottom of the reservoir and forms a water cone invading the gas well. Excessive early water production can even lead to well shutdown. As development progresses, the edge water continues to invade the gas well along the highly developed fracture zones, and the water production of the well shows

a rapid increase after recompletion. Therefore, it can be summarized as a bottom cone transverse invasion pattern.

The distribution characteristics of fractures in fracture-pore reservoirs have an impact on the water invasion pattern. When fractures are not connected to the bottom water, water first enters the medium/large pores in the matrix and then enters the fractures. When fractures are connected to the bottom water, water first enters the fractures, and after the fractures are filled with water, water invades the medium/large pores in the matrix. In fracture-pore reservoirs, invading water cannot enter small pores because of the strong capillary force in small pores, making it difficult for water to enter them. Due to the low resistance of fractures and medium/large pores, invading water will preferentially enter these spaces, forming dominant flow channels. Water invades along these channels and prevents water from entering small pores. The rapid infiltration of formation water along the fracture development zone into the interior of the gas reservoir is manifested as a fracture water invasion pattern.

5. Conclusions

1. A pore compressibility factor testing method for a full-diameter core saturated with kerosene under reservoir conditions, with constant confining pressure and variable porosity fluid pressure, was established in the laboratory. This method eliminates the influence of the experimental medium, kerosene, on the pore compressibility factor. The experimental conditions better simulate the actual gas reservoir conditions. It was found that the pore compressibility factor is minimally affected by pressure and remains relatively constant at approximately 0.00085/MPa.
2. The static method, which solely relies on static parameters to calculate the influx index, suffers from limitations in evaluating water energy, making it difficult to accurately determine water body multiples. This greatly affects the results obtained with the static method and makes it challenging to match the results with those obtained using the dynamic method. By comparing the results obtained using the static and dynamic methods, dynamically adjusting the dynamic reserve and water body multiples values, and iteratively revising the pore compressibility factor using a bisection method, the static and dynamic method results were made consistent. This method improves the reliability of influx index evaluation for water-invasion gas reservoirs.
3. Using the example of the Kela-2 gas field, the combined static/dynamic iterative method was applied to calculate a dynamic reserve of 235 billion m^3 and a water body multiple of 4.8. The influx index gradually decreased with decreasing formation pressure, but the magnitude of change was not significant. Overall, it remained above 0.3, with an average of 0.35, indicating that the Kela-2 gas field belongs to the category of strong water-invasion gas reservoirs.

Author Contributions: W.X.; methodology, T.J.; software, S.G.; validation, H.L.; formal analysis, L.Y.; investigation, W.Z.; resources, W.A.; data curation, D.H.; writing—original draft preparation, D.H.; writing—review and editing, D.H.; visualization, D.H.; supervision, D.H.; project administration, W.X.; funding acquisition, W.X. All authors have read and agreed to the published version of the manuscript.

Funding: This research was funded by [the project of the Recovery Factor of Different Types of Gas Reservoirs and Mechanisms for Improving the Recovery Factor of the Science Research and Technology Development Project of the China National Petroleum Corporation grant number [2021DJ1701].

Data Availability Statement: Data is unavailable due to privacy or ethical restrictions.

Conflicts of Interest: The authors declare no conflicts of interest. Author Jiangtongwen was employed by the Department of Science and Technology Management, PetroChina Company Limited. The remaining authors declare that the research was conducted in the absence of any commercial or financial relationships that could be construed as a potential conflict of interest".

Nomenclature

WEDI	Influx index, dimensionless
W_e	Cumulative water invasion, 10^4 m^3
G_p	Cumulative gas production, 10^4 m^3
W_p	Cumulative water production, 10^4 m^3
B_g	Gas volumetric factor, dimensionless
B_w	Formation water volumetric factor, dimensionless
G	Dynamic reserves, 10^4 m^3
B_{gi}	Gas volumetric factor at the original reservoir pressure, dimensionless
ΔV_r	Compressibility volume of rock pores, 10^4 m^3
G_pB_g	Underground volumes of cumulative gas production, m^3
W_pB_w	Volumes of cumulative water production, m^3
$G\ (B_g - B_{gi})$	Expansion volumes of natural gas, m^3
ΔV_w	Expansion volumes of bound water, m^3
ΔV_r	Volumes pore compressibility, m^3
C_w	Reservoir water compressibility factor, mpa^{-1}
C_f	Pore compressibility factor, mpa^{-1}
S_{wi}	Represent the initial water saturation, %
P_e	Effective pressure, in mpa
P_{gf}	Overburden pressure, mpa
P	Formation fluid pressure, in mpa
ρ	Density of the overburden rock, g/cm^3
h	Thickness of the overburden reservoir, m
C_{fe}	Experimentally measured comprehensive pore compressibility factor, mpa^{-1}
Δm_k	Kerosene oil production, g
ρ_k	Density of kerosene, g/cm^3
V_p	Pore volume of the rock core, cm^3
p	Pore pressure, mpa
C_{fk}	Compressibility factor of kerosene, mpa^{-1}
V_s	Initial pumped liquid volume, ml
V_o	Final pumped liquid volume, ml
Δp	Pressure difference before and after the rigid container experiment, mpa
C_f	Pore compressibility factor, mpa^{-1}
β	Water body multiple
V_w	Water body volume, m^3
V_o	Gas reservoir volume, m^3
I_1	Gas displacement index, dimensionless
I_2	Rock and connate water displacement index, dimensionless
p_i	Original formation pressure, mpa;
P_j	Reservoir pressure at any arbitrary time point
B	Water influx constant m^3/d,
t_j	Reservoir production time, d
Δp	Pressure drop across the water body, mpa
$Q_d\ (t_D)$	Dimensionless water influx
t_D	Dimensionless production time
W_{ei}	The initial water that can be encroached in place at initial pressure p_i, m^3

Appendix A. Experimental Apparatus

A testing method for the pore compressibility factor under reservoir conditions was established in the laboratory (Figure 2). The intermediate container (2000 mL) was used to contain kerosene. A pressure up to 60 MPa was supplied by one ISCO booster pump (Lincoln, TX, USA). The gas flowmeter (ABB, Zurich, Switzerland) was applied to accurately measure gas flow rate. The casing pressure pump (Haskel, Burbank, CA, USA) was used for supplying liquids or gases under high pressure.

References

1. Golmohammadi, M.; Mahani, H.; Ayatollahi, S. Toward low-salinity waterflooding predictive capability development in carbonates for fast screening of oil-brine-rock candidates. *Geoenergy Sci. Eng.* **2023**, *221*, 111258. [CrossRef]
2. Liu, S.; Zhang, Y.; Du, H.; Liu, J.; Zhou, Z.; Wang, Z.; Huang, K.; Pan, B. Experimental study on fluid flow behaviors of waterflooding fractured-vuggy oil reservoir using two-dimensional visual model. *Phys. Fluids* **2023**, *35*, 212396.
3. Chu, F.; Zhang, X.; Zhang, G.; Dong, C. Deep learning prediction of waterflooding-based alteration of reservoir hydraulic flow unit. *Geoenergy Sci. Eng.* **2023**, *231*, 212396. [CrossRef]
4. Saw, R.K.; Mandal, A. Experimental investigation on fluid/fluid and rock/fluid interactions in enhanced oil recovery by low salinity water flooding for carbonate reservoirs. *Fuel* **2023**, *352*, 129156.
5. Karimpour Khamaneh, M.; Mahani, H. Pore-Scale Insights into the Nonmonotonic Effect of Injection Water Salinity on Wettability and Oil Recovery in Low-Salinity Waterflooding. *Energy Fuels* **2023**, *37*, 14764–14777. [CrossRef]
6. Mokhtari, R.; Nick, H.M.; Farhadzadeh, M.; Feilberg, K.L. Role of sulfate ion on wettability alteration and oil mobilization in chalk reservoirs during modified salinity waterflooding. *Geoenergy Sci. Eng.* **2023**, *227*, 211922. [CrossRef]
7. Khormali, A.; Ahmadi, S. Prediction of barium sulfate precipitation in dynamic tube blocking tests and its inhibition for waterflooding application using response surface methodology. *J. Pet. Explor. Prod. Technol.* **2023**, *13*, 2267–2281. [CrossRef]
8. Hosseinzadehsadati, S.; Bonto, M.; Mokhtari, R.; Eftekhari, A.A.; Feilberg, K.L.; Nick, H.M. Modified salinity waterflooding in chalk reservoirs: A journey from rock and fluid interfaces to field scale applications. *Fuel* **2024**, *356*, 129461. [CrossRef]
9. Schilthuis, R.J. Active oil and reservoir energy. *Trans. AIME* **1936**, *118*, 33–52. [CrossRef]
10. Van Everdingen, A.F.; Hurst, W. The application of the Laplace transformation to flow problems in reservoirs. *J. Pet. Technol.* **1949**, *1*, 305–324. [CrossRef]
11. Fetkovich, M.J. A simplified approach to water influx calculations-finite aquifer systems. *J. Pet. Technol.* **1971**, *23*, 814–828. [CrossRef]
12. Li, C. *Principles of Reservoir Engineering*, 2nd ed.; Petroleum Industry Press: Beijing, China, 2011; pp. 124–183.
13. Zhu, Y.X.; Xie, X.L.; Luo, K. Analysis of factors influencing production characteristics of Kela 2 overpressured gas field. *Pet. Explor. Dev.* **2001**, *28*, 60–63.
14. Sun, H.; Ouyang, W.; Zhu, S.; Wan, Y.; Tang, Y.; Cao, W. A new numerical well test method of multi-scale discrete fractured tight sandstone gas reservoirs and its application in the Kelasu Gas Field of the Tarim Basin. *Nat. Gas Ind. B* **2023**, *10*, 103–113. [CrossRef]
15. Bruns, J.R.; Fetkvoich, M.J.; Meitzen, V.C. The effect of water influx on p/z-cumulative gas production curves. *J. Pet. Technol.* **1965**, *17*, 287–291. [CrossRef]
16. Xue, X.; Chen, G.; Zhang, K.; Zhang, L.; Zhao, X.; Song, L.; Wang, M.; Wang, P. A divide-and-conquer optimization paradigm for waterflooding production optimization. *J. Pet. Sci. Eng.* **2022**, *211*, 110050. [CrossRef]
17. Jiang, Z.; Liu, Z.; Zhao, P.; Chen, Z.; Mao, Z. Evaluation of tight waterflooding reservoirs with complex wettability by NMR data: A case study from Chang 6 and 8 members, Ordos Basin, NW China. *J. Pet. Sci. Eng.* **2022**, *213*, 110436. [CrossRef]
18. Wang, N.; Huang, B.; Zhang, C. A novel method of calculating water-flooded gas in place and water influx of water drive gas reservoirs. *J. Southwest Pet. Univ. Sci. Technol. Ed.* **2000**, *22*, 26–27.
19. Tang, S.; Luo, D.; Yan, Z.; Liu, Y.J.; Xu, Q.H.; Jiang, P.; Li, X.Y. A new method of calculating the reserves of gas reservoirs strongly driven by edge and bottom water in the eastern South China Sea. *Nat. Gas Ind.* **2013**, *33*, 44–47.
20. Zhang, X.; Liu, W.H. Method for Calculating Dynamic Reserves of Water Drive Gas Reservoir with Considering of Water-sealing Gas. *Appl. Mech. Mater.* **2014**, *522*, 1542–1546. [CrossRef]
21. Sharma, H.; Mohanty, K.K. Modeling of low salinity waterflooding in carbonates: Effect of rock wettability and organic acid distribution. *J. Pet. Sci. Eng.* **2022**, *208*, 109624. [CrossRef]
22. Zeng, X.; Zhang, W.; Chen, T.; Jacobsen, H.A.; Zhou, J.; Chen, B. Evaluating interwell connectivity in waterflooding reservoirs with graph-based cooperation-mission neural networks. *SPE J.* **2022**, *27*, 2443–2452. [CrossRef]
23. Hall, H.N. Compressibility of reservoir rocks. *J. Pet. Technol.* **1953**, *5*, 17–19. [CrossRef]
24. Zhang, X.; Su, Y.; Li, L.; Da, Q.; Hao, Y.; Wang, W.; Liu, J.; Gao, X.; Zhao, A.; Wang, K. Microscopic remaining oil initiation mechanism and formation damage of CO_2 injection after waterflooding in deep reservoirs. *Energy* **2022**, *248*, 123649. [CrossRef]
25. Zhang, T.; Tang, M.; Ma, Y.; Zhu, G.; Zhang, Q.; Wu, J.; Xie, Z. Experimental study on CO_2/Water flooding mechanism and oil recovery in ultralow-Permeability sandstone with online LF-NMR. *Energy* **2022**, *252*, 123948. [CrossRef]
26. Dake, L.P. The practice of reservoir engineering. *J. Pet. Sci. Eng.* **1994**, *14*, 263.
27. Farahani, M.; Aghaei, H.; Saki, M.; Asadolahpour, S.R. Prediction of pore volume compressibility by a new non-linear equation in carbonate reservoirs. *Energy Geosci.* **2022**, *3*, 290–299. [CrossRef]
28. Soltanmohammadi, R.; Iraji, S.; de Almeida, T.R.; Basso, M.; Munoz, E.R.; Vidal, A.C. Investigation of pore geometry influence on fluid flow in heterogeneous porous media: A pore-scale study. *Energy Geosci.* **2024**, *5*, 100222. [CrossRef]
29. Cai, J.; Tang, Q.; Ou, J.; Yuan, Q.; Deng, Z.; Gan, X. Flow mass balance in over-pressured gas reservoirs considering water influx. *Fault-Block Oil Gas Field* **2019**, *26*, 596–600.
30. Chai, R.; Liu, Y.; He, Y.; Liu, Q.; Xue, L. Dynamic behaviors and mechanisms of fluid-fluid interaction in low salinity waterflooding of carbonate reservoirs. *J. Pet. Sci. Eng.* **2022**, *208*, 109256. [CrossRef]

31. Tian, Z.; Wei, W.; Zhou, S.; Sun, C.; Rezaee, R.; Cai, J. Impacts of gas properties and transport mechanisms on the permeability of shale at pore and core scale. *Energy* **2022**, *244*, 122707. [CrossRef]
32. Fan, S.; Liu, G.; Xue, H.; Zhang, X.; Liu, H. How pore structure evolves in shale gas extraction: A new fractal model. *Gas Sci. Eng.* **2023**, *117*, 205061. [CrossRef]
33. Delavar, M.R.; Ramezanzadeh, A. Pore pressure prediction by empirical and machine learning methods using conventional and drilling logs in carbonate rocks. *Rock Mech. Rock Eng.* **2023**, *56*, 535–564. [CrossRef]
34. Li, J.H.; Li, B.B.; Cheng, Q.Y.; Gao, Z. Characterization of the fracture compressibility and its permeability for shale under the effects of proppant embedment and compaction: A preliminary study. *Pet. Sci.* **2022**, *19*, 1125–1138. [CrossRef]
35. Han, X.; Shan, S.; Xu, G.; Han, Y.; Guo, Y.; Yang, B.; Zhang, J.; Yao, P.; Chu, X.; Zhang, P. Single-and Multifractal Dimension Variation of the Pore-Fracture System in Tight Sandstone by Using High-Pressure Mercury Intrusive Tests and Its Influence on Porosity–Permeability Variation. *Energy Fuels* **2023**, *37*, 11969–11981. [CrossRef]
36. Hou, X.; Zhu, Y.; Wang, Y.; Liu, Y. Experimental study of the interplay between pore system and permeability using pore compressibility for high rank coal reservoirs. *Fuel* **2019**, *254*, 115712. [CrossRef]
37. Miao, Z.; Fu, X.; Duan, C.; Li, Y. Influencing factor analysis of the coal matrix compressibility of middle-high rank coals. *J. Nat. Gas Sci. Eng.* **2020**, *81*, 103462. [CrossRef]